High-frequency fluctuations of a modulated, helical electron beam

M. A. Reynolds[a] and G. J. Morales
Department of Physics and Astronomy, University of California, Los Angeles, California 90095

(Received 17 June 1996; accepted 27 August 1996)

The high-frequency electromagnetic field generated by a density-modulated, helical electron beam propagating in a magnetized plasma is calculated. The magnetic fluctuations are found to exhibit spatially localized (evanescent) resonances at harmonics of the electron-cyclotron frequency, whose width is determined by the pitch angle of the beam, and whose existence is a consequence of the helical geometry. In addition, electrostatic modes are radiated near the hybrid frequencies, and electromagnetic modes are radiated above the upper-hybrid frequency. The predicted frequency spectrum and mode structure in configuration space are in good agreement with experimental observations of discrete emission lines at the electron-cyclotron harmonics [Phys. Fluids B **5**, 3789 (1993)]. © *1996 American Institute of Physics.* [S1070-664X(96)01312-2]

I. INTRODUCTION

There are several areas of contemporary plasma physics in which radiation from localized charge distributions plays an important role. Current and temperature filaments in tokamaks,[1] auroral electron beams in the ionosphere,[2] and artificial particle beams injected into space[3] are some of these areas.

This analytical study is motivated by a laboratory experiment performed by Stenzel and Golubyatnikov[4] at the University of California, Los Angeles (UCLA), in which the properties of the fluctuating magnetic field near a helical electron beam in a high-density magnetized plasma were measured. This is a fundamental experiment which explores the source of fluctuations near the harmonics of the electron-cyclotron frequency, and a theoretical understanding is necessary to lay the foundation for more involved studies and applications. When the plasma is weakly magnetized ($\Omega_e \ll \omega_{pe}$, where Ω_e and ω_{pe} are the electron-cyclotron and the electron-plasma frequencies, respectively), the observed frequency spectrum of the axial component of the magnetic field is characterized by sharp resonances at the harmonics of Ω_e.[4] Resonances of this type have been observed previously, e.g., remotely by Landauer,[5] but not *in situ* as in the UCLA experiment. These local measurements show that no plasma instability or nonlinearity is involved, but that the fields are generated by the free-streaming electrons. That is, large fields are produced only when the condition $\omega - n\Omega_e = k_\parallel U_\parallel$ is satisfied, where $U_\parallel$ is the velocity of the beam parallel to the magnetic field and n is the azimuthal mode number.

Previous theoretical work on linear fields has focused on propagating modes and has not examined the evanescent fields which characterize the parameter regime of the UCLA experiment. For example, there has been long-standing interest in the space-physics community in the problem of modulated electron beams acting as sources of whistler waves.[3] Lavergnat *et al.*[6–9] studied Bernstein modes, plasma waves and electromagnetic whistler waves generated by beams injected into the ionosphere. They included realistic beam effects, such as a beam front and the fact that the beam has a finite thickness on the order of the Brillouin radius. Harker and Banks[10,11] calculated the power radiated by a helical electron beam through the far field, and also the explicit form of the near field. However, they restricted their study to the whistler and lower-hybrid frequency regimes, and also to a square-wave density modulation. This type of modulation allows certain integrals to be evaluated analytically, but hinders the understanding of the intrinsic frequency spectrum of the beam (which must be multiplied by the spectrum of the modulation to obtain the radiated spectrum).

Another motivation for the study of localized beams is the explanation of laboratory experiments like those of Landauer[5] where many harmonics of Ω_e are observed in the frequency spectrum of the fields measured outside of the plasma chamber. Canobbio and Croci[12] were among the first to suggest single-particle radiation as a possible explanation for Landauer's experiment. They considered the radiation of electron Bernstein modes by a single electron in a hot plasma and found enhanced emission at the upper-hybrid frequency, but did not determine how these quasi-electrostatic waves could convert to the electromagnetic radiation observed by Landauer.

In addition to treating all frequency regimes equally, the present study considers the density modulation to be arbitrary, and separates out those effects that are due to the geometry of the beam from those that are due to the details of the modulation. Also, while the general formulation allows for either ion or electron beams, this study concentrates on electron beams and frequencies above Ω_e. It is found that the resonances observed by Stenzel and Golubyatnikov[4] are due to the helical geometry of the beam, which forces variations in z to be mapped into variations in θ, and which produces large fields only for the beam modes, $\omega - n\Omega_e = k_\parallel U_\parallel$. In the frequency regime $\Omega_e < \omega < \omega_{pe}$ the plasma modes are evanescent in the perpendicular direction so that the fields are localized near the beam. Near the hybrid frequencies, however, the plasma modes propagate and are electrostatic in character, in agreement with the findings of Canobbio.[13] Finally, for frequencies above ω_{pe}, the plasma is essentially transparent near the electron-cyclotron harmon-

[a]Present address: Beam Physics Branch, Plasma Physics Division, Naval Research Laboratory, Washington, D.C. 20375.

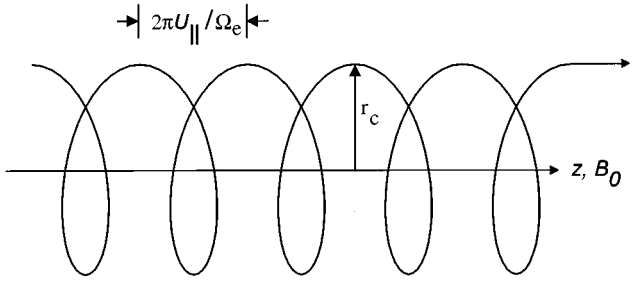

FIG. 1. Geometry of the helical beam considered in the analysis.

ics, and the beam radiates electromagnetic fields similar to those in a vacuum.

Section II formulates the general helical beam problem, and sketches the calculation of the fields produced by that beam. Section III examines in detail the physics of the high-frequency regime ($\omega > \Omega_e$) and catalogues the character of the fields, including the sharp resonances at the electron-cyclotron harmonics in the frequency spectrum. The analytical predictions are compared with experimental observations in Sec. IV, and Sec. V is the conclusion.

II. CALCULATION OF FIELDS

The source of the fluctuations is modeled as a density-modulated, charged-particle beam of infinite extent in the z direction, immersed in a uniform plasma with a background magnetic field $\mathbf{B}_0 = B_0 \hat{\mathbf{z}}$. The role of this beam is that of a current source; no plasma feedback is included in this formulation, and hence no instabilities. Effects due to the injection point and beam front are not crucial to the form of the steady-state fields, and hence are not included. However, the beam is defined by its properties at the $z=0$ plane, as if it were injected at that point. To facilitate future study of different types of beams within one theoretical description, we consider beams whose current density $\mathbf{j}_b(\mathbf{x},t)$ is proportional to a radial δ-function

$$\mathbf{j}_b(\mathbf{x},t) \propto \delta(\rho - r_c), \tag{1}$$

where ρ is the usual cylindrical radial coordinate and r_c is the cyclotron radius of the beam particles. This formulation is able to describe single particles, helical beams, and annular beams. All three types have the property that the particles remain at a fixed radius $\rho = r_c$.

The experimental realization of this model consists of a beam injected continuously into the plasma at a specific location, and at a given angle to the ambient magnetic field, as sketched in Fig. 1. This beam spirals along the magnetic field and, because the modulation affects only the density, it retains its helical shape; there is no velocity spread. Let n be the number of particles per-unit-length in the z direction at time t and position z; because the particles simply free stream in the z direction, n is a function only of $\tau \equiv t - z/U_{\|}$. The total current passing through the $z=0$ plane (i.e., ''injected'') per-unit-time is given by $qn(t)U_{\|}$, where q is the single-particle charge. In the cylindrical coordinates of configuration space (ρ, θ, z) the beam current density has only $\hat{\theta}$ and $\hat{\mathbf{z}}$ components

$$\mathbf{j}_b(\mathbf{x},t) = \frac{nq}{r_c}(U_{\|}\hat{\mathbf{z}} + \Omega_e r_c \hat{\theta})\,\delta(\rho - r_c)\,\delta(\theta - \Omega_e z/U_{\|}), \tag{2}$$

where $\Omega_e = qB_0/m_e c$ and m_e is the mass of the beam electrons. A relativistic correction may be included in Ω_e if the beam's velocity is large enough; however, in this paper we restrict our study to beam velocities which are nonrelativistic. Alternatively, the perpendicular velocity, $U_{\perp} \equiv \Omega_e r_c$, can be used to parametrize the beam. The Fourier transform [i.e., assuming a dependence of $\exp(ik_{\|}z - i\omega t + in\theta)$] of the helical current in Eq. (2) is

$$\tilde{\mathbf{j}}_b(\rho, n, k_{\|}, \omega) = \frac{2\pi c q \tilde{n}}{r_c}\left[\frac{U_{\|}}{c}\hat{\mathbf{z}} + \frac{\Omega_e r_c}{c}\hat{\theta}\right] \times \delta\left(k_{\|} - \frac{\omega - n\Omega_e}{U_{\|}}\right)\delta(\rho - r_c), \tag{3}$$

where

$$\tilde{n} = \int_{-\infty}^{\infty} d\tau\, e^{i\omega\tau} n(\tau) \tag{4}$$

is the spectrum of the modulation at $z=0$ (the ''injection'' point).

The formalism can be extended to the other two types of beams mentioned previously: single particles and annular beams. The only modifications appear in the expressions for n and $\tilde{n}$. For a single particle, the density becomes a δ-function and its transform is a constant

$$n = \delta(z - U_{\|}t), \quad \tilde{n} = \frac{1}{U_{\|}}. \tag{5}$$

For an annular beam, the beam density must be integrated over the angle θ' at which the beam crosses the $z=0$ plane. That is, n is a function of both τ and θ', and $\tilde{n}$ is a function of both frequency ω and azimuthal mode number n

$$\tilde{n}(\omega, n) = \int_{-\infty}^{\infty} d\tau\, e^{i\omega\tau} \int_0^{2\pi} d\theta'\; e^{in\theta'} n(\tau, \theta'). \tag{6}$$

The Fourier transforms of the current density of all three types of beams have the same structure due to the fact that they are made up of free-streaming particles. The particle nature of the source current is manifested in Eq. (3), which holds for all three types; only the correct expression for $\tilde{n}$ must be inserted [Eq. (4), (5) or (6)].

The calculation of the linear electric and magnetic fields due to a current source with cylindrical symmetry in a cold plasma is similar to the derivation of the fields in a uniform waveguide,[14] but must be modified for a tensor dielectric.[15] Because the technique is well-known and straightforward, only a sketch is given.

The plasma is represented by the cold dielectric tensor

$$\varepsilon = \begin{bmatrix} \epsilon_{\perp} & -i\epsilon_H & 0 \\ i\epsilon_H & \epsilon_{\perp} & 0 \\ 0 & 0 & \epsilon_{\|} \end{bmatrix}, \tag{7}$$

where the elements of ε are functions of ω only. The separation of the fields into parallel and perpendicular components (with respect to $\hat{\mathbf{z}}$, the direction of the static magnetic

field) decouples Maxwell's equations, resulting in differential equations for the parallel field components, E_z and B_z. The solutions away from the beam are written in terms of Bessel functions, and then integrated over the source to obtain the overall magnitude of the fields. The perpendicular field components can then be determined in terms of the parallel components if desired. This method works when the medium is uniform and can be described by a scalar dielectric.[14] It is also applicable to tensor media when, as in the present case, the dielectric tensor is both Hermitean and block diagonal.[15]

The complete solution for the parallel electric and magnetic fields is

$$E_z(\mathbf{r},\omega)=\frac{q\tilde{n}}{r_c}e^{i\omega z/U_\parallel}\sum_n e^{in(\theta-\Omega_e z/U_\parallel)} \times\sum_{\pm}\begin{Bmatrix} h_\pm J_n(k_\pm\rho) & \rho<r_c \\ j_\pm H_n^{(1)}(k_\pm\rho) & \rho>r_c\end{Bmatrix}, \tag{8a}$$

$$B_z(\mathbf{r},\omega)=\frac{q\tilde{n}}{r_c}e^{i\omega z/U_\parallel}\sum_n e^{in(\theta-\Omega_e z/U_\parallel)} \times\sum_{\pm}\eta_\pm\begin{Bmatrix} h_\pm J_n(k_\pm\rho) & \rho<r_c \\ j_\pm H_n^{(1)}(k_\pm\rho) & \rho>r_c\end{Bmatrix}, \tag{8b}$$

where

$$\begin{Bmatrix} h_\pm \\ j_\pm\end{Bmatrix}=\frac{-\pi i}{\epsilon_\perp(\eta_\pm-\eta_\mp)}\left[k_\pm r_c\epsilon_\perp\frac{U_\perp}{c}\begin{Bmatrix} H_n^{(1)\prime}(k_\pm r_c) \\ J_n'(k_\pm r_c)\end{Bmatrix} -\left(k_0 r_c[N_\parallel\epsilon_H-i\eta_\mp(\epsilon_\perp-N_\parallel^2)]\frac{U_\parallel}{c} +n[\epsilon_H+i\eta_\mp N_\parallel]\frac{U_\perp}{c}\right)\begin{Bmatrix} H_n^{(1)}(k_\pm r_c) \\ J_n(k_\pm r_c)\end{Bmatrix}\right]. \tag{9}$$

Here, J_n and $H_n^{(1)}$ are Bessel functions and Hankel functions of the first kind, respectively, the prime denotes differentiation with respect to their argument, $N_\parallel=(\omega-n\Omega_e)/k_0U_\parallel$ is the scaled parallel wave number, $k_0=\omega/c$, and

$$\eta_\pm=\frac{\epsilon_\perp(k_\pm^2/k_0^2)-\epsilon_\parallel(\epsilon_\perp-N_\parallel^2)}{i\epsilon_H N_\parallel} =\frac{i\epsilon_H N_\parallel\epsilon_\parallel}{\epsilon_\perp(\epsilon_\perp-N_\parallel^2)-\epsilon_H^2-\epsilon_\perp(k_\pm^2/k_0^2)}. \tag{10}$$

The quantity $k_\pm$ is the perpendicular wave number, and is given by the two solutions of the dispersion relation

$$(\epsilon_\parallel-N_\perp^2)[(\epsilon_\perp-N^2)(\epsilon_\perp-N_\parallel^2)-\epsilon_H^2]-N_\perp^2N_\parallel^2(\epsilon_\perp-N^2)=0, \tag{11}$$

where $N^2=N_\perp^2+N_\parallel^2$ and $N_\perp^2=k_\pm^2/k_0^2$. The fields may alternatively be expressed in terms of the modified Bessel functions I_n and K_n by making the replacements

$$H_n^{(1)}(k_\pm r_c)J_n(k_\pm\rho)\rightarrow\frac{2i}{\pi}K_n(\kappa_\pm r_c)I_n(\kappa_\pm\rho), \tag{12a}$$

$$J_n(k_\pm r_c)H_n^{(1)}(k_\pm\rho)\rightarrow\frac{2i}{\pi}I_n(\kappa_\pm r_c)K_n(\kappa_\pm\rho), \tag{12b}$$

where $\kappa_\pm^2=-k_\pm^2$. When the character of the fields is primarily evanescent, the modified Bessel functions provide a more convenient form for both interpretation and numerical evaluation.

The perpendicular components of the electric and magnetic fields are linear combinations of the parallel components, and can be determined by applying the operator $\hat{\mathbf{z}}\times$ to Ampère's law and Faraday's law to obtain

$$\boldsymbol{\nabla}_\perp B_z-ik_\parallel\mathbf{B}_\perp+ik_0\hat{\mathbf{z}}\times\boldsymbol{\varepsilon}\cdot\mathbf{E}_\perp=0, \tag{13a}$$

$$\boldsymbol{\nabla}_\perp E_z-ik_\parallel\mathbf{E}_\perp-ik_0\hat{\mathbf{z}}\times\mathbf{B}_\perp=0, \tag{13b}$$

where $\boldsymbol{\nabla}_\perp=\boldsymbol{\nabla}-\hat{\mathbf{z}}\partial/\partial z$. Equations (13) can be solved algebraically for $\mathbf{E}_\perp$ and $\mathbf{B}_\perp$ in $k_\parallel$ space, and the resulting expressions inverse-transformed if configuration-space dependence is desired.

III. GENERAL FIELD BEHAVIOR

Equations (8) are now evaluated for an electron beam and for frequencies above Ω_e. For weak magnetic fields ($\Omega_e<\omega_{pe}$) this range of frequencies consists of three regimes: the ''evanescent'' regime ($\Omega_e<\omega<\omega_{pe}$) where the fields are radially localized, the ''upper-hybrid'' regime ($\omega_{pe}<\omega<\omega_{uh}$) where the beam excites propagating upper-hybrid waves, and the ''vacuum'' regime ($\omega_{uh}<\omega$) where the beam excites propagating electromagnetic modes near the harmonics of Ω_e. When the magnetic field is strong ($\omega_{pe}<\Omega_e$) only the last two of these regimes exist above Ω_e.

Before evaluating the fields numerically, it is helpful to investigate the physics qualitatively by examining the structure of Eqs. (8). All of the field components, for example B_z, may be written in the dimensionless form

$$\overline{B_z}(\mathbf{r},\omega)\equiv\frac{B_z}{(q\tilde{n}/r_c)}=\sum_n b_{zn}(\rho,\omega)e^{iz(\omega-n\Omega_e)/U_\parallel}e^{in\theta}, \tag{14}$$

where b_{zn} is the strength of the nth term. An investigation of $\overline{B_z}$ (rather than B_z) has the advantage of separating the effects of the density modulation, $\tilde{n}$, from those inherent to the beam. The dependence of the nth term on θ and z is oscillatory

$$\exp(in\theta)\exp\left[iz\left(\frac{\omega-n\Omega_e}{U_\parallel}\right)\right]. \tag{15}$$

This structure arises as a consequence of the beam geometry, which demands that if the azimuthal dependence is harmonic, $\exp(in\theta)$, then the axial dependence is a phase oscillation due to the free streaming, i.e., only those waves which satisfy the Doppler-shifted cyclotron condition

$$\omega-n\Omega_e=k_\parallel U_\parallel, \tag{16}$$

are excited. The strength of the nth term is governed by $b_{zn}(\rho,\omega)$, whose evaluation requires a detailed knowledge of the dispersion relation because it depends sensitively on $k_\pm$.

The parallel index of refraction $N_\parallel$ is a measure of the frequency separation from the nth harmonic

$$N_\parallel \propto \omega - n\Omega_e . \tag{17}$$

Two limits are useful: $N_\parallel \approx 0$ (near the nth harmonic) and $N_\parallel \to \infty$ (far from the nth harmonic). In the small $N_\parallel$ limit, the two solutions for the perpendicular wave number are approximated by

$$N_\perp^2 \approx \epsilon_\parallel , \quad \frac{\epsilon_\perp^2 - \epsilon_H^2}{\epsilon_\perp}, \tag{18}$$

which are the well-known dispersion relations for the ordinary and extraordinary modes, respectively. For large $N_\parallel$, $N_\perp^2$ approaches

$$N_\perp^2 \to -N_\parallel^2 , \quad -\frac{\epsilon_\parallel}{\epsilon_\perp} N_\parallel^2 , \tag{19}$$

which are the dispersion relations for the electromagnetic and electrostatic modes, respectively. In Eq. (19), $N_\parallel$ has been taken to be larger than all elements of the dielectric, which means the frequency does not correspond to a hybrid resonance.

There are three important dimensionless parameters: the pitch angle

$$\theta_p = \tan^{-1}(U_\perp / U_\parallel), \tag{20}$$

the scaled velocity

$$\beta = \frac{\sqrt{U_\parallel^2 + U_\perp^2}}{c}, \tag{21}$$

and the effective magnetization

$$\alpha = \frac{\omega_{pe}^2}{\Omega_e^2}. \tag{22}$$

A. Evanescent regime: $\Omega_e < \omega < \omega_{pe}$

In this frequency regime, the real part of $N_\perp^2$ is negative for all values of $N_\parallel$, hence the fields are radially evanescent and are localized near the beam. We will show that each term in Eq. (14) decays exponentially as the frequency is varied away from cyclotron harmonics. Figure 2 shows a typical spectrum, $\overline{B_z}(\omega)$, for a beam with a pitch angle of $\theta_p = 88°$ and a scaled velocity of $\beta = 0.01$, immersed in a plasma of $\alpha = 10^4$. This spectrum is taken at the spatial location of $\rho/r_c = 0.7$ and $\theta = z = 0$. It is convenient to choose $z = 0$ because, except for the phase factor due to the free-streaming [see Eq. (15)], the field is periodic in z with a period of $2\pi U_\parallel / \Omega_e$. All figures in this paper will therefore evaluate the fields at $z = 0$. Peaks occur at the cyclotron harmonics, with a maximum amplitude that decreases with increasing harmonic number. To understand this spectrum, each term in Eq. (14) needs to be considered in more detail.

Near the nth harmonic, the nth term in the sum is larger than the other terms and has the shape of a resonance, with exponential wings. To illustrate this feature, consider ω to be different from $n\Omega_e$. In this case, $N_\parallel$ is large, the asymptotic solutions in Eq. (19) may be used, and the strength of the nth term approaches the value

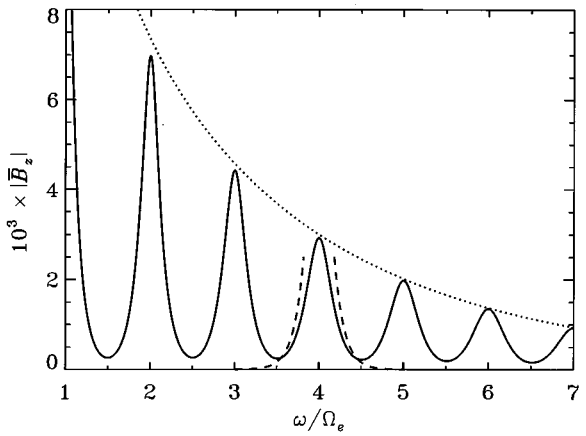

FIG. 2. Frequency spectrum of the scaled magnetic field $\overline{B_z}$. The spatial location is $\rho/r_c = 0.7$, $\theta = z = 0$, the beam parameters are $\theta_p = 88°$, $\beta = 0.01$, and $\omega_{pe}^2/\Omega_e^2 \equiv \alpha = 10^4$. The choice of $z = 0$ is a convenience, and is made in all of the figures. The dashed line is Eq. (23) for $n = 4$ and the dotted line is Eq. (26).

$$b_{zn} \to \frac{U_\perp}{c}\sqrt{\frac{r_c}{\rho}}\exp(-k_\parallel|\rho - r_c|), \tag{23}$$

where the exponential behavior stems from the large argument expansion of the radial Bessel functions. The approximation in Eq. (23) is shown as a dashed line in Fig. 2 for the $n = 4$ term. To determine the frequency scale, the argument of the exponential can be written in the form

$$k_\parallel|\rho - r_c| = \frac{|\omega - n\Omega_e|}{\Delta}, \tag{24}$$

where

$$\frac{\Delta}{\Omega_e} \equiv \frac{(U_\parallel / U_\perp)}{|1 - \rho/r_c|} = \frac{\cot\,\theta_p}{|1 - \rho/r_c|}, \tag{25}$$

is defined as the width of the resonance, corresponding to one e-folding. For the values of the parameters in Fig. 2, Eq. (25) predicts a half-width of $\Delta/\Omega_e = 0.12$, in good agreement with Fig. 2. Sharp resonances, therefore, are obtained at radial locations far from the beam ($\rho/r_c \to \infty$ or $\rho/r_c \approx 0$), and for large pitch angles. For large pitch angles, Eq. (25) implies that the resonance width depends sensitively on θ_p. This dependence is depicted in Fig. 3 which shows the frequency spectrum for three values of the pitch angle, $\theta_p = 87°$, 88°, and 89°, and at the same spatial location as Fig. 2 ($\rho/r_c = 0.7$ and $\theta = z = 0$). The determination of the resonance width as a function of ρ is complicated by the fact that the magnitude of the field is also a function of radial position, as is investigated next.

When ω is near a harmonic, $N_\parallel \approx 0$, and Eq. (18) can be used to approximate the perpendicular wave number. If, in addition, ρ is not too large, the Bessel functions may be expanded for small argument to approximate the magnitude of the field at the peak of the nth harmonic

$$b_{zn} \approx -\frac{U_\perp}{c}\frac{1}{\epsilon_\perp}\begin{Bmatrix} (\epsilon_H + \epsilon_\perp)(\rho/r_c)^n & \rho < r_c \\ (\epsilon_H - \epsilon_\perp)(r_c/\rho)^n & \rho > r_c \end{Bmatrix}. \tag{26}$$

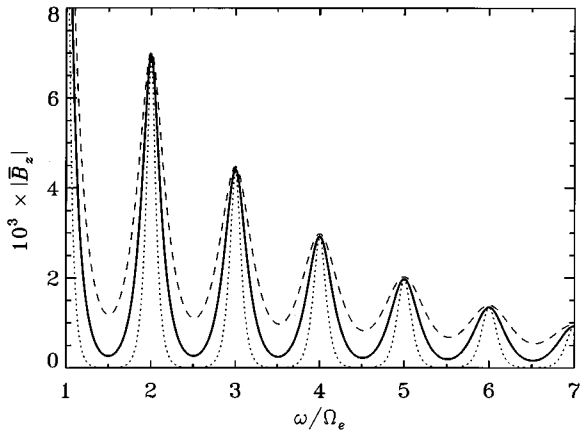

FIG. 3. Frequency spectrum of the scaled magnetic field $\overline{B_z}$ for three different values of the pitch angle $\theta_p = 87°$ (dashed line), 88° (solid line), and 89° (dotted line). The spatial location is $\rho/r_c = 0.7$, $\theta = z = 0$, the beam velocity is $\beta = 0.01$, and $\alpha = 10^4$.

This is due solely to the extraordinary mode, for the polarization of the ordinary mode is $B_z = E_\theta = 0$. This expression contains both the decrease of peak amplitude with harmonic number n for a given radial position, shown as the dotted line in Fig. 2, as well as the dependence of peak amplitude on ρ/r_c for a given harmonic number. The radial dependence of $\overline{B_z}$ for $\omega = 2\Omega_e$ and for three different values of the azimuthal angle, $\theta = 0°$, 90°, and 180°, is shown in Fig. 4. Far from $\rho = r_c$, the fields are well-approximated by a power law in ρ, as predicted by Eq. (26). Of course, as ρ becomes large, the small-argument expansion is no longer valid, and the fields become evanescent. Near the cyclotron radius, the width of the harmonic resonances increases, implying that many terms contribute significantly to the sum, and the radial dependence departs from the simple power law. This is the mathematical manifestation of the fact that the induced plasma current near the beam is strong and has a complex spatial structure.

The following picture emerges:

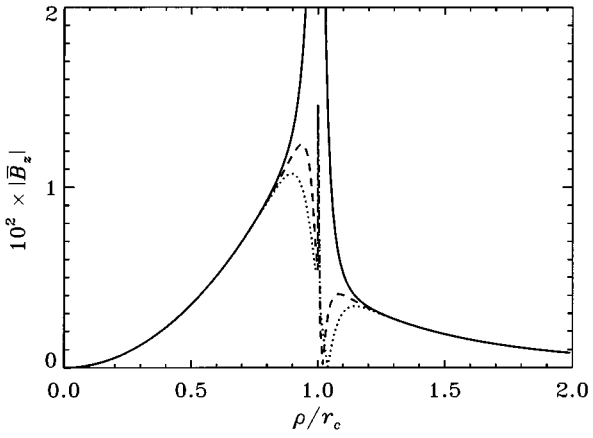

FIG. 4. Radial dependence of the scaled magnetic field $\overline{B_z}$ for three different values of azimuthal angle $\theta = 0°$ (solid line), 90° (dashed line), and 180° (dotted line). The parameters are $\omega/\Omega_e = 2$, $\beta = 0.01$, $\alpha = 10^4$, and $\theta_p = 88°$.

(1) Each term in the sum has axial and azimuthal dependence given by Eq. (15), and a radial dependence given by Eq. (26) at the harmonic, and by Eq. (23) far from the harmonic.
(2) For large pitch angles and far from the radial location of the beam, the frequency spectrum consists of sharp resonances at the cyclotron harmonics. In this parameter regime, these resonances are well-approximated by one term in the infinite sum — the other terms are exponentially small. Hence, the field has the same spatial dependence as the single, dominant, term.
(3) Close to the radial location of the beam, $\rho \approx r_c$, and for small pitch angles, many terms contribute significantly to the magnitude of the field. In this case, the field magnitude at a given frequency is a superposition of those terms that are ''closest,'' in the sense of Eq. (17).

These properties are due to the Bessel functions which appear in the expression for the field, and hence are a consequence of the helical geometry. Because all components of **E** and **B** depend on this same product of Bessel functions, they all exhibit similar structure.

B. Upper-hybrid regime: $\omega_{pe} < \omega < \omega_{uh}$

This frequency regime is characterized by electrostatic wave propagation. As long as ω_{pe} and ω_{uh} are far from the harmonics of Ω_e, the value of $N_\parallel$ is large for all terms in the sum, the approximation in Eq. (19) can be used, and because the electrostatic mode has a real and positive $N_\perp^2$, the fields propagate. Although the dispersion relation is well approximated by the electrostatic dispersion relation, $k_\perp^2 \epsilon_\perp + k_\parallel^2 \epsilon_\parallel = 0$, the fields have a significant magnetic component, hence we continue to use B_z as characteristic of the field structure. The electromagnetic mode may be ignored because it is evanescent with a short decay length $L \equiv k_\perp^{-1} \ll r_c$, where the inequality is due to the fact that $k_\perp \sim N_\parallel$.

To illustrate the behavior in the upper-hybrid regime, we choose the value of $\alpha = 20.25$, which implies $\omega_{pe} = 4.5\Omega_e$ and $\omega_{uh} \approx 4.61\Omega_e$. This upper-hybrid regime corresponds to the frequency interval between the $n = 4$ and $n = 5$ harmonics so that the large $N_\parallel$ approximation is appropriate for all terms in the infinite sum. Figure 5 shows the magnetic field due to the $n = 5$ and $n = 6$ terms at a radial position of $\rho = 2r_c$, outside of the beam. The oscillations in the field are due to the Bessel functions $J_5(k_- r_c)$ and $J_6(k_- r_c)$, where $k_- \approx k_0 N_\parallel \sqrt{-\epsilon_\parallel/\epsilon_\perp}$. As ω approaches ω_{uh}, $\epsilon_\perp$ approaches zero, and the oscillations are more closely spaced. The field in this limit approaches the value

$$|b_{zn}| \to 2N_\parallel^2 \frac{U_\parallel}{c} \sqrt{\frac{r_c}{\rho}} \sqrt{\left|\frac{\epsilon_\parallel}{-\epsilon_\perp}\right|} \left|\cos\left(k_- r_c - \frac{1}{2} n\pi - \frac{1}{4}\pi\right)\right|. \tag{27}$$

Because these waves propagate away from the beam, it is useful to discuss the power radiated by the beam and its radiation resistance. The total power radiated per-unit-length P may be found by integrating the Poynting vector **S** over a cylinder of length L and radial position $\rho \gg r_c$ that is centered on the beam

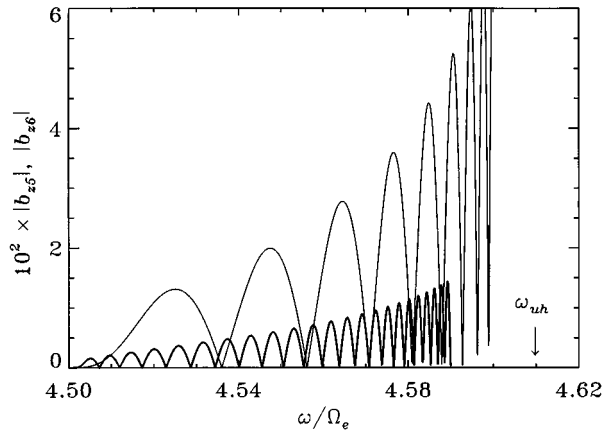

FIG. 5. Frequency dependence of b_{z5} (thin line) and b_{z6} (thick line) for the parameter values of $\alpha=20.25$, $\beta=0.01$, $\theta_p=88°$, and a spatial location $\rho/r_c=2$, $\theta=z=0$.

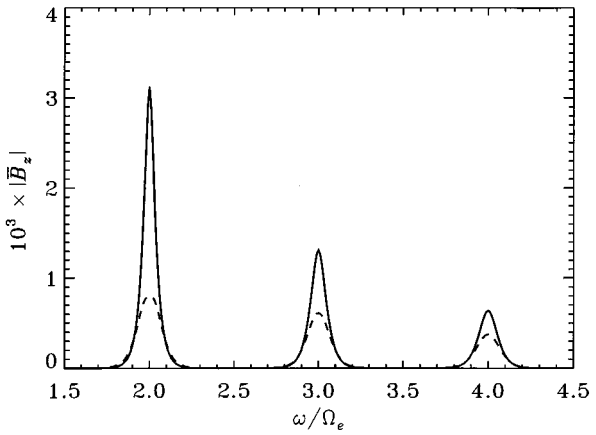

FIG. 6. Frequency spectrum of the scaled magnetic field $\overline{B_z}$ in the vacuum regime. The spatial location is $\rho/r_c=2$, $\theta=z=0$, and the parameters are $\beta=0.01$, $\theta_p=88°$, and $\alpha=1$. For comparison, the dashed line is the spectrum for $\alpha=10^4$, with all other parameters the same.

$$P=\frac{1}{L}\int_0^L dz\int_0^{2\pi} d\theta\ \rho S_\rho . \tag{28}$$

The contributions from the endcaps of the cylinder cancel. A radiation resistance per-unit-length, which is a measure of the efficiency of the beam, may be defined as

$$R\equiv\frac{2}{|I|^2}P, \tag{29}$$

where $|I|^2=q^2U_\parallel^2|\tilde{n}|^2$. In this upper-hybrid frequency regime, the resistance is approximately

$$R\approx\sum_n \frac{2N_\parallel}{cr_c}\frac{1}{\sqrt{-\epsilon_\parallel\epsilon_\perp}}\cos^2\left(k_-r_c-\frac{1}{2}n\pi-\frac{1}{4}\pi\right). \tag{30}$$

For the parameters in Fig. 5, the magnitude of each term is approximately

$$\frac{2N_\parallel}{cr_c}\approx 1.2\times 10^{-4}n\Omega_e\frac{\text{ohm}}{\text{cm}}, \tag{31}$$

if Ω_e is measured in s^{-1}. Electrostatic waves are also radiated above the lower-hybrid frequency.

C. Vacuum regime: $\omega_{uh}<\omega$

For frequencies larger than the upper-hybrid frequency, $N_\perp^2$ can be real and positive for small values of $N_\parallel^2$, i.e., the ordinary mode propagates for $\omega>\omega_{pe}$, while the extraordinary mode propagates for $\omega>\omega_{uh}$. This implies that for frequencies very near the nth harmonic, the nth term describes a propagating electromagnetic field. The contribution of other terms is exponentially small because for them $N_\parallel^2$ is large.

To illustrate this behavior, we choose $\alpha=1$ which places all harmonics above the upper-hybrid frequency, so that both modes will propagate for small $N_\parallel$. A typical near-field spectrum is shown in Fig. 6, for $\rho/r_c=2$, $\beta=0.01$, and $\theta_p=88°$. Also shown is the spectrum for $\alpha=10^4$ (evanescent regime) for comparison. As in the evanescent regime, sharp resonances occur because the parameter Δ/Ω_e is small, and the strength of each term decays exponentially. However, the beam radiates near the cyclotron harmonics, and the radiation resistance per-unit-length is again a useful quantity. Unlike the upper-hybrid regime, the regions in frequency space corresponding to propagation do not overlap for different n, so that the radiation resistance per-unit-length for $\omega=n\Omega_e$ (on the harmonics) becomes

$$R=\frac{\pi\omega}{U_\parallel^2}\left[\left(\frac{U_\parallel}{c}\right)^2 J_n^2(k_+r_c)+\frac{\Omega_e^2/\omega^2}{\epsilon_\perp(\epsilon_\perp^2-\epsilon_H^2)}\right.$$
$$\left.\times\{n\epsilon_H J_n(k_-r_c)-k_-r_c\epsilon_\perp J_n'(k_-r_c)\}^2\right], \tag{32}$$

where

$$k_+r_c=n\frac{U_\perp}{c}\epsilon_\parallel, \tag{33a}$$

$$k_-r_c=n\frac{U_\perp}{c}\frac{\epsilon_\perp^2-\epsilon_H^2}{\epsilon_\perp}. \tag{33b}$$

The two terms in the square brackets represent the power radiated into the ordinary mode and extraordinary mode, respectively.

As ω becomes large compared with ω_{pe}, the radiated fields closely approximate those that would be radiated by a beam in vacuum. That is, ε approaches $\mathbf{1}$ in this high-frequency limit, and the arguments of the Bessel functions approach $nU_\perp/c$. If $U_\perp/c\ll 1$ as well, i.e., the beam is nonrelativistic, the radiation resistance takes a simple form

$$R\approx\frac{\pi n\Omega_e}{U_\parallel^2}\frac{\left(\frac{1}{2}n\frac{U_\perp}{c}\right)^{2n}}{(n!)^2}\left[\left(\frac{U_\parallel}{c}\right)^2+n^4\left(\frac{U_\perp}{c}\right)^4\right], \tag{34}$$

which for large n becomes

$$R(n\to\infty)\to\frac{\pi n\Omega_e}{U_\parallel^2}\left(\frac{e}{2}\frac{U_\perp}{c}\right)^{2n}, \tag{35}$$

so that the resistance decreases with harmonic number as β^{2n}, as expected.

IV. COMPARISON WITH EXPERIMENT

In the experiment performed at UCLA by Stenzel and Golubyatnikov,[4] the parallel component of the fluctuating magnetic field is measured using a $\dot{B}$ probe, which consists of a circular wire coil in which the induced emf driven by the changing magnetic flux through the loop is detected. The $\dot{B}$ probe is 2.3 cm in radius, with a thickness of 2.6 mm. This radius is approximately equal to the cyclotron radius of the beam electrons, the exact ratio depending on the beam's perpendicular velocity. The background plasma in which the beam is immersed is weakly magnetized, $\Omega_e \ll \omega_{pe}$, and its temperature is low enough to warrant the approximation of the dielectric tensor by that of a cold plasma.

There are three experimental facts which, when contrasted with the theoretical idealization presented here, make the quantitative comparison between experiment and theory difficult. First, and most important, is the finite size of the $\dot{B}$ probe. The experimental technique cannot detect variations in the magnetic field on a scale smaller than the size of the probe. For typical beam energies of 30 V–100 V, the corresponding cyclotron radii are $r_c \approx 1.7$ cm–3 cm. This means that the probe is not much smaller than the beam, and is sometimes larger. The present theory, however, determines the field locally. Because of the mathematical form in which we have expressed the fields (an infinite sum of Bessel functions), it is difficult to integrate the field over the area of the probe, except when the probe is located either completely inside the beam ($\rho < r_c$) or completely outside ($\rho > r_c$). Second, while the theory singles out a specific pitch angle and beam velocity, the experimental beam has a finite spread in these quantities produced by the broadband noise inherent in the injection process. Thus, there is no well-defined beam axis. Third, the beam is injected from a specific location and does not extend infinitely in z. This fact leads to the experimental observation that when the probe is near the injection point, the field spectrum is broadband, corresponding to the noise of the injection. However, when the probe is far from the injection point, those modes that are not coherent are filtered out, and spectra more closely resembling those in Fig. 2 are obtained. This implies that the theory can only be used to explain measurements taken far from the disturbing influence of the injector.

The simple axial and azimuthal dependence predicted by Eq. (15) is observed using interferometric techniques. For large pitch angles ($\theta_p \approx 88°$) and frequencies near Ω_e and its first harmonic ($\omega/\Omega_e = 1,2$), the observed θ dependence is clearly $e^{in\theta}$ and the measured z dependence is uniform, i.e., $k_\parallel = 0$. The phase change in z is also measured for intermediate frequencies ($\Omega_e \leqslant \omega \leqslant 2\Omega_e$) and $k_\parallel$ is found to be consistent with Eq. (16), where n is the ''closest'' harmonic, i.e., due to that term which has the largest magnitude. The present theory agrees well with these observations.

The observed radial dependence at the first harmonic ($\omega/\Omega_e = 2$), depicted in Fig. 12 of Ref. 4, also is in agreement with the present theory as shown in Fig. 7. This theoretical plot is a cut along x for $y = 0$. That is, negative values of x correspond to $\theta = 180°$ while positive values signify $\theta = 0°$. The minimum at $x = 0$ and the decay for $|x| > r_c$

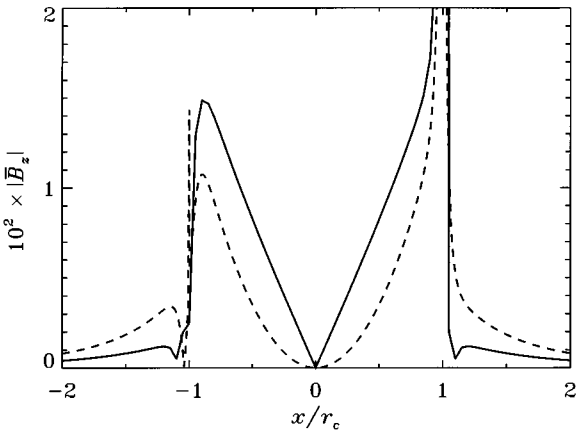

FIG. 7. Radial dependence of the scaled magnetic field $\overline{B_z}$ (theoretical prediction) for the first two harmonics $\omega/\Omega_e = 1.01$ (solid line) and $\omega/\Omega_e = 2$ (dashed line). The parameters are $\theta_p = 88°$, $\beta = 0.01$, $z = 0$, and $\theta = 0°$, 180°. Compare with Fig. 12 of Ref. 4.

shown in Fig. 7 is seen in the experiment. However, the measured field decreases more slowly, a feature expected from the finite size of the probe. At the cyclotron frequency ($\omega = \Omega_e$), however, there is a significant discrepancy. While the experimental measurement does show a sharp drop in magnitude for $\rho \geqslant r_c$, it remains large for $\rho < r_c$ and does not show a minimum at $\rho = 0$. The present theory does not predict this type of behavior, most likely because it does not include any dissipation mechanisms which might be present in the experiment.

The frequency dependence of the magnetic fluctuations is perhaps the most striking result of the experiment, and is explained by the present theory. The theoretical spectrum in Fig. 8, where the parameters were chosen to approximate the experimental conditions, agrees qualitatively with the experimental spectrum seen in Fig. 6 of Ref. 4. A quantitative comparison is difficult to make, for the reasons mentioned earlier. Due to the dependence of the resonance width on pitch angle and radial location, and the experimental spread in these quantities, the resonances of the observed spectra

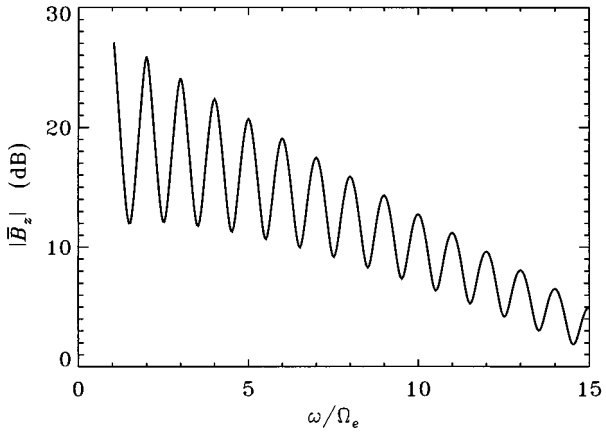

FIG. 8. Frequency spectrum of the scaled magnetic field $\overline{B_z}$. The spatial location is $\rho/r_c = 0.7$, $\theta = z = 0$, and the parameters are $\theta_p = 88°$, $\beta = 0.0198$, and $\alpha = 8711$. Compare with Fig. 6 of Ref. 4.

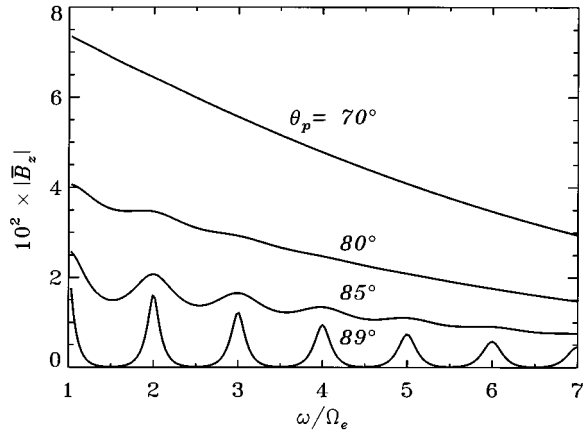

FIG. 9. Dependence of the frequency spectrum of the scaled magnetic field $\overline{B_z}$ on the pitch angle θ_p of the beam. The parameters are $\beta=0.0198$, $\alpha=10^4$, and the spatial location is $\rho/r_c=0.7$, $\theta=z=0$. Compare with Fig. 8 of Ref. 4.

have a minimum width, regardless of the average parameters of the beam. A clear dependence of resonance width on pitch angle is indeed observed in the experiments (see Fig. 8 of Ref. 4). The sensitivity of the experimental resonance width on θ_p, however, is not as strong as predicted by the present model. Figure 9 shows that the resonances disappear when $\theta_p \approx 80°$, while experimentally they are seen for pitch angles as small as 70°. Because experimentally, the resonance width depends strongly on the distance between the probe and the injection point, and, since this is not addressed in the present theory, it is difficult to offer an explanation for the discrepancy. However, it is worth noting that while a general tendency is for the non-ideal experimental realities to destroy theoretically sharp features, in this case the observed behavior is contrary to this trend.

The linear beam modes excited by spiraling electrons, as calculated by the present theory, agree qualitatively with the experimental results. Some of the discrepancies can be understood in light of the method of measurement, i.e., a spatial integration of B_z rather than a localized measurement, and by taking into account the experimental limitations and the theoretical idealizations. However, the two points of disagreement are puzzling: the radial structure for $\omega=\Omega_e$, and the resonance width for small pitch angles.

V. CONCLUSION

The electromagnetic fluctuation spectrum generated by a modulated, free-streaming, helical electron beam has been calculated and compared to a recent laboratory experiment.[4] For the frequency regime of the experiment ($\Omega_e < \omega \ll \omega_{pe}$), the spectrum consists of localized, evanescent fields which shows a series of sharp resonances at the electron-cyclotron harmonics. This behavior is well described by the excitation of beam modes which satisfy the condition $\omega - n\Omega_e = k_\parallel U_\parallel$. The width and magnitude of these resonant peaks can be explained by the form of the fields both near the harmonics and far from the harmonics. It is found that the peaks are functions of the pitch angle and the spatial location. The axial and azimuthal dependence of the fields is also described by the model developed in this study. A discrepancy arises between the experimental results and the theoretical prediction for the radial dependence of the field at Ω_e. The finite size of the measuring instrument, a magnetic loop which integrates the flux, as well as the idealization of the theory, which includes neither a velocity modulation nor a spread in pitch angle, are the probable causes for the discrepancy.

In addition, the present theoretical formulation is general enough to describe fluctuations generated in other frequency regimes as well as those generated by ion beams. This generality allows the calculation of quantities such as the radiated power in a straightforward manner, without resorting to approximations. Two of these other frequency regimes, near and above the upper-hybrid frequency ω_{uh}, have been considered. Near ω_{uh} the beam radiates a broad spectrum of electrostatic waves which propagate away from the beam, and propagating electromagnetic modes are emitted near those harmonics of Ω_e that are above ω_{uh}.

ACKNOWLEDGMENTS

We thank Professor R. Stenzel for illuminating discussions concerning his experimental results.

This work is sponsored by the Office of Naval Research.

[1] N. J. Lopes Cardozo, F. C. Schuller, C. J. Barth, C. C. Chu, F. J. Pijper, J. Lok, and A. A. M. Oomens, Phys. Rev. Lett. **73**, 256 (1994).
[2] J. E. Maggs, in *Artificial Particle Beams in Space Plasma Studies*, edited by B. Grandal (Plenum, New York, 1982), p. 261.
[3] T. Neubert and P. M. Banks, Planet. Space Sci. **40**, 153 (1992).
[4] R. L. Stenzel and G. Golubyatnikov, Phys. Fluids B **5**, 3789 (1993).
[5] G. Landauer, J. Nucl. Energy C (Plasma Phys.) **4**, 395 (1962).
[6] J. Lavergnat and R. Pellat, J. Geophys. Res. **84**, 7223 (1979).
[7] J. Lavergnat and R. Pellat, in Ref. 2, p. 535.
[8] J. Lavergnat and T. Lehner, IEEE Trans. Antennas Propag. **AP-32**, 177 (1984).
[9] J. Lavergnat, T. Lehner, and G. Matthieussent, Phys. Fluids **27**, 1632 (1984).
[10] K. J. Harker and P. M. Banks, Planet. Space Sci. **33**, 953 (1985).
[11] K. J. Harker and P. M. Banks, Planet. Space Sci. **35**, 11 (1987).
[12] E. Canobbio and R. Croci, Phys. Fluids **9**, 549 (1966); R. Croci and E. Canobbio, in *Proceedings of the Seventh International Conference on Phenomena in Ionized Gases, Beograd, 1965*, edited by B. Perovic and D. Tosic (Gradevinska Knjiga, Beograd, 1966), Vol. II, p. 496.
[13] E. Canobbio, Nucl. Fusion **1**, 172 (1961).
[14] J. D. Jackson, *Classical Electrodynamics*, 2nd ed. (Wiley, New York, 1975), Sec. 8.2.
[15] W. P. Allis, S. J. Buchsbaum, and A. Bers, *Waves in Anisotropic Plasmas* (MIT Press, Cambridge, MA, 1963), Chap. 9.